Subgrid Methods for Resolving Axial Heterogeneity in Planar Synthesis Solutions for the Boltzmann Transport Equation

Ph.D. Defense

Aaron M. Graham

July 20, 2017

- Predicting the neutron flux distribution is crucial for reactor analysis
- The flux distribution determines the power distribution, which has important ramifications for design and operation
  - Economically, efficient fuel loading patterns and prevention of fuel failures are determined largely by the power distribution
  - The power distribution also drives safety constraints for both steady-state and transient operation, including accident scenarios
- These requirements demand a high degree of accuracy from the codes used in reactor analysis

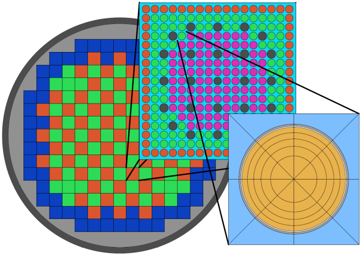

- Reactor analysis has traditionally used a two-step approach
  - Lattice calculations to generate homogenized cross sections
  - Nodal diffusion methods to solve global problem with homogenized cross sections
- Recent increases in computing power have generated interest in direct, whole-core transport calculations
  - Monte Carlo
  - Deterministic 3D transport
  - Planar Synthesis Methods: 2D/1D and 2D/3D

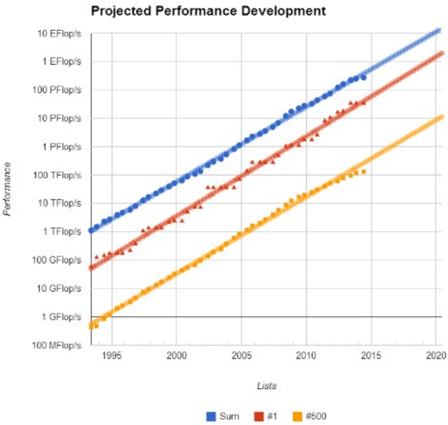

- Planar synthesis methods are faster than 3D transport, but still computationally expensive
- To make these methods useful practically, runtimes need to be decreased
  - Algorithm and methods improvements
  - Reduction in number of planes
- Subgrid methods can be used to maintain accuracy with fewer planes
  - Needs to be able to capture local effects of various reactor components
  - Should be able to be applied to a variety of situations
  - Cheaper than using more planes
- Three new methods developed to accomplish two goals:
  - Significant reduction in errors caused by control rod cusping, the most severe axial heterogeneity for planar synthesis methods
  - Reduce the runtime of the 2D/1D code MPACT for cases with rod cusping

Boltzmann Transport Equation

$$
\begin{aligned}
&\frac{1}{v}\frac{\partial\varphi}{\partial t} + \boldsymbol{\Omega}\cdot\boldsymbol{\nabla}\varphi + \Sigma_t\left(\boldsymbol{x}, E, t\right)\varphi\left(\boldsymbol{x}, E, \boldsymbol{\Omega}, t\right) \\
&= \frac{1}{4\pi}\int_0^\infty\int_{4\pi}\Sigma_s\left(\boldsymbol{x}, E' \to E, \boldsymbol{\Omega}' \to \boldsymbol{\Omega}\right)\varphi\left(\boldsymbol{x}, E', \boldsymbol{\Omega}'\right) d\Omega' dE' \\
&\quad + \frac{\chi_p\left(\boldsymbol{x}, E\right)}{4\pi}\int_0^\infty\int_{4\pi}\left(1 - \beta\left(\boldsymbol{x}, E'\right)\right)\nu\Sigma_f\left(\boldsymbol{x}, E', t\right)\varphi\left(\boldsymbol{x}, E', \boldsymbol{\Omega}', t\right) d\Omega' dE' \\
&\quad + \sum_{j=1}^{N_d}\frac{\chi_{d,j}\left(\boldsymbol{x}, E\right)}{4\pi}\lambda_j C_j\left(\boldsymbol{x}, t\right) + Q\left(\boldsymbol{x}, E, \boldsymbol{\Omega}, t\right)
\end{aligned}
$$

$$
\varphi\left(\boldsymbol{x}_b, E, \boldsymbol{\Omega}, t\right) = \varphi^b\left(\boldsymbol{x}_b, E, \boldsymbol{\Omega}, t\right) \ , \quad \boldsymbol{\Omega}\cdot\boldsymbol{n} < 0 \qquad \text{(1a)}
$$

Boltzmann Transport Equation

- Transport equation is continuous in space, time, energy and angle
- For this work, only the steady-state eigenvalue form of the equation is considered
- Multigroup approximation is used to discretize in energy
- Discrete ordinates (S_N) approximation is applied to discretize in angle, using an angular quadrature to integrate the angular flux φ

Steady-State Transport Equation

$$\begin{aligned}\boldsymbol{\Omega}_n \cdot \nabla \varphi_{g,n} + \Sigma_{t,g}\left(\boldsymbol{x}\right)\varphi_{g,n}\left(\boldsymbol{x}\right) &= \frac{1}{4\pi}\sum_{g'=1}^{G}\sum_{n'=1}^{N}\Sigma_{g'\to g,n'\to n}\left(\boldsymbol{x}\right)\varphi_{g',n'}\left(\boldsymbol{x}\right)w_{n'} \\ &+ \frac{1}{k_{eff}}\frac{\chi_g}{4\pi}\sum_{g'=1}^{G}\sum_{n'=1}^{N}\nu\Sigma_{f,g'}\left(\boldsymbol{x}\right)\varphi_{g',n'}\left(\boldsymbol{x}\right)w_{n'}\end{aligned}$$

$$\varphi_{g,n}\left(\boldsymbol{x}_b\right) = \varphi_g^b\left(\boldsymbol{x}_b, \boldsymbol{\Omega}_n\right) \;, \quad \boldsymbol{\Omega}_n \cdot \boldsymbol{n} < 0$$

- Calculations discussed here use transport-correction isotropic scattering (TCP_0) to simplify the scattering source

Diffusion Approximation

- Assumes linearly anisotropic flux and relationship between scalar flux ϕ and current J

$$\psi_g\left(\boldsymbol{x},\boldsymbol{\Omega}\right) \approx \frac{1}{4\pi}\left(\phi_g\left(\boldsymbol{x}\right) + 3\boldsymbol{\Omega}\cdot\boldsymbol{J}_g\left(\boldsymbol{x}\right)\right)$$

$$\boldsymbol{J}\left(\boldsymbol{x}\right) \approx -\boldsymbol{D}\left(\boldsymbol{x}\right)\boldsymbol{\nabla}\phi\left(x\right)$$

$$\boldsymbol{D}\left(\boldsymbol{x}\right) = \frac{1}{3}\left(\Sigma_{tr,g}\left(\boldsymbol{x}\right)\right)^{-1}$$

- Eliminates angle dependence, simplifies streaming and scattering source terms

$$-\boldsymbol{\nabla}\cdot\boldsymbol{D}_g\left(\boldsymbol{x}\right)\boldsymbol{\nabla}\phi\left(\boldsymbol{x}\right) + \Sigma_{t,g}\left(\boldsymbol{x}\right)\phi_g\left(\boldsymbol{x}\right) = \sum_{g'=1}^{G}\Sigma_{s0,g'\to g}\left(\boldsymbol{x}\right)\phi_{g'}\left(\boldsymbol{x}\right)$$

$$+\frac{1}{k_{eff}}\frac{\chi_g}{4\pi}\sum_{g'=1}^{G}\nu\Sigma_{f,g'}\left(\boldsymbol{x}\right)\phi_{g'}\left(\boldsymbol{x}\right) + Q_g\left(\boldsymbol{x}\right)$$

Background

- 2D/1D method was developed by researchers at Korea Atomic Energy Research Institute (KAERI) [1, 2, 3]
  - Takes advantage of reactor geometry
  - High fidelity transport radially with faster, lower order method axially

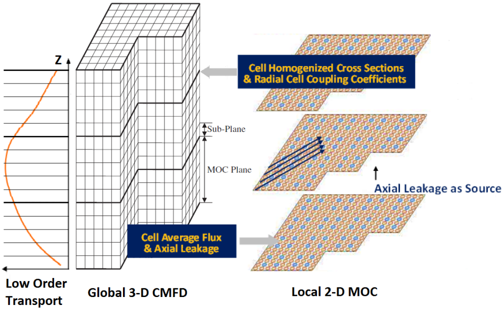

- Newer 2D/1D code MPACT, jointly developed by University of Michigan and Oak Ridge National Laboratory, is used for this work

Radial Equations

- Average transport equation axially from $z_{k-\frac{1}{2}}$ to $z_{k+\frac{1}{2}}$
- Assume cross sections are axially constant in region of integration

$$\Omega_x \frac{\partial \psi_g^Z}{\partial x} + \Omega_y \frac{\partial \psi_g^Z}{\partial y} + \Sigma_{tr,g}(x,y)\,\psi_g^Z(x,y,\boldsymbol{\Omega}) = q_g^Z(x,y,\boldsymbol{\Omega}) + L_g^Z(x,y,\Omega_z)$$

$$q_g^Z(x,y,\boldsymbol{\Omega}) = \frac{1}{4\pi}\sum_{g'=1}^{G}\int_{4\pi}\Sigma_{s,g'\to g}^Z\left(x,y,\boldsymbol{\Omega}'\cdot\boldsymbol{\Omega}\right)\psi_{g'}^Z\left(x,y,\boldsymbol{\Omega}'\right)d\Omega'$$
$$+\frac{1}{k_{eff}}\frac{\chi_g^Z}{4\pi}\sum_{g'=1}^{G}\int_{4\pi}\nu\Sigma_{f,g'}^Z(x,y)\,\psi_{g'}^Z\left(x,y,\boldsymbol{\Omega}'\right)d\Omega' + \frac{Q_g^Z(x,y)}{4\pi}$$

$$L_g^Z(x,y,\Omega_z) = \frac{\Omega_z}{\Delta z_k}\left(\psi_{g,z_{k-\frac{1}{2}}} - \psi_{g,z_{k+\frac{1}{2}}}\right) \approx \frac{J_{g,z_{k-\frac{1}{2}}} - J_{g,z_{k+\frac{1}{2}}}}{4\pi\Delta z_k}$$

Axial Equations

- Average transport equation over x from $x_{i-\frac{1}{2}}$ to $x_{i+\frac{1}{2}}$ and over y from $y_{j-\frac{1}{2}}$ to $y_{j+\frac{1}{2}}$
- Assume cross sections are radially constant in region of integration

$$\Omega_z \frac{\partial \psi_g^{XY}}{\partial z} + \Sigma_{tr,g}^{XY}(z)\,\psi_g^{XY}(z,\mathbf{\Omega}) = q_g^{XY}(z,\mathbf{\Omega}) + L_g^{XY}(z,\Omega_x,\Omega_y)$$

$$L_g^{XY}(z,\Omega_x,\Omega_y) \approx \frac{J_{g,x_{i-\frac{1}{2}},y_j} - J_{g,x_{i+\frac{1}{2}},y_j}}{4\pi\Delta x_i} + \frac{J_{g,x_i,y_{j-\frac{1}{2}}} - J_{g,x_i,y_{j+\frac{1}{2}}}}{4\pi\Delta y_j}$$

Calculation Flow

- 3D CMFD [4]
  - Determines global flux shape to scale fine mesh solution
  - Calculates radial currents for 1D axial solver
- 1D NEM-P_3 [5, 6]
  - Calculates improved axial currents for 2D solver
- 2D MOC [7, 8]
  - Solves for fine mesh scalar flux
  - Calculates updated radial currents for CMFD calculation

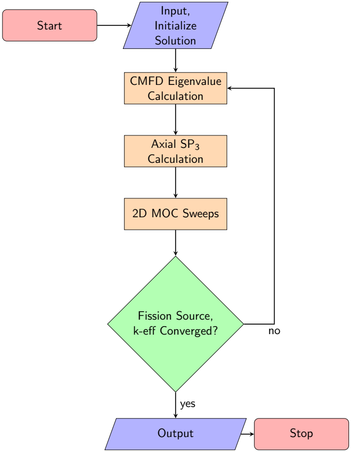

3D CMFD

- Diffusion-based acceleration performed on coarse mesh
- $\hat{D}$ coupling coefficients enforce consistency between diffusion and transport solutions

$$\hat{D}_{g,s} = \frac{J_{g,s}^{trans,k-1} + \tilde{D}_{g,s}\left(\phi_{g,p}^{diff,k} - \phi_{g,m}^{diff,k}\right)}{\left(\phi_{g,p}^{trans,k} + \phi_{g,m}^{diff,k}\right)}$$

- Coarse mesh solution projected to fine mesh solution, preserving MOC radial shape and CMFD volume-averaged flux

$$\phi_{g,j}^{MOC,k} = \frac{\phi_{g,i}^{CMFD,k}}{\phi_{g,i}^{CMFD,k-1}} \phi_{g,j}^{MOC,k-1}$$

- Subplane scheme is used to capture subplane axial flux shapes

1D NEM-P_3

- P_3 [5] used to handle angular shape

$$-\nabla\cdot D_{0,g}(\boldsymbol{x})\nabla\Phi_{0,g}(\boldsymbol{x})+[\Sigma_{tr,g}(\boldsymbol{x})-\Sigma_{s0,g}(\boldsymbol{x})]\Phi_{0,g}(\boldsymbol{x})$$
$$=Q_g(\boldsymbol{x})+2[\Sigma_{tr,g}(\boldsymbol{x})-\Sigma_{s0,g}(\boldsymbol{x})]\Phi_{2,g}(\boldsymbol{x})$$

$$-\nabla\cdot D_{2,g}(\boldsymbol{x})\nabla\Phi_{2,g}(\boldsymbol{x})+[\Sigma_{tr,g}(\boldsymbol{x})-\Sigma_{s2,g}(\boldsymbol{x})]\Phi_{2,g}(\boldsymbol{x})$$
$$=\tfrac{2}{5}\{[\Sigma_{tr,g}(\boldsymbol{x})-\Sigma_{s0,g}(\boldsymbol{x})][\Phi_{0,g}(\boldsymbol{x})-2\Phi_{2,g}(\boldsymbol{x})]-Q_g(\boldsymbol{x})\}$$

- NEM [6] used to handle spatial shape

$$Q(\xi)=\sum_{i=0}^{2} q_i P_i(\xi)\ ,\quad \phi(\xi)=\sum_{i=0}^{4} \phi_i P_i(\xi)$$

$$\int_{-1}^{1} P_n(\xi)\left(-\frac{D}{h^2}\frac{d^2}{d\xi^2}\phi(\xi)+\Sigma_r\phi(\xi)-Q(\xi)\right)d\xi=0,\ n=0,1,2$$

$$\phi_L(1)=\phi_R(-1)\ ,\quad J_L(1)=J_R(-1)$$

2D MOC

- Solve along a specific direction Ω_n to reduce the problem from a PDE to an ODE that can be solved analytically

$$\frac{\partial\psi_{g,n}}{\partial s}+\Sigma_{t,g}(\boldsymbol{r}_0+s\boldsymbol{\Omega}_n)\psi_{g,n}(\boldsymbol{r}_0+s\boldsymbol{\Omega}_n)=q_{g,n}(\boldsymbol{r}_0+s\boldsymbol{\Omega}_n)$$

$$\begin{aligned}\psi_{g,n}(\boldsymbol{r}_0+s\boldsymbol{\Omega}_n) =&\psi_{g,n}(\boldsymbol{r}_0)\exp\left(-\int_0^s \Sigma_{t,g}(\boldsymbol{r}_0+s'\boldsymbol{\Omega}_n)ds'\right)\\ &+\int_0^s q_{g,n}(\boldsymbol{r}_0+s'\boldsymbol{\Omega}_n)\exp\left(-\int_0^{s'} \Sigma_{t,g}(\boldsymbol{r}_0+s''\boldsymbol{\Omega}_n)ds''\right)ds'\end{aligned}$$

- Assume flat source, cross section along track with length L_j and spacing δx

$$\begin{aligned}\psi^{out}_{g,i,n,j}&=\psi^{in}_{g,i,n,j}e^{-\Sigma_{t,g,i}L_j}+\frac{q_{g,i,n}}{\Sigma_{t,g,i}}\left(1-e^{-\Sigma_{t,g,i}L_j}\right)\\ \overline{\psi}_{g,i,n,j}&=\frac{q_{g,n,i}}{\Sigma_{t,g,i}}+\frac{1-e^{-\Sigma_{t,g,i}L_j}}{L_j\Sigma_{t,g,i}}\left(\psi^{in}_{g,i,n,j}-\frac{q_{g,n,i}}{\Sigma_{t,g,i}}\right)\\ \overline{\psi}_{g,i,n}&=\frac{\sum_j\overline{\psi}_{g,i,n,j}\delta x L_j}{\sum_j \delta x L_j}\end{aligned}$$

2D MOC

- Perform ray tracing and store segment information up front
- Set up scattering, fission, and axial transverse leakage sources
  - Multi-group sweeping
  - 1-group sweeping
- Parallel Decomposition
  - Spatial (Planar and Radial)- MPI
  - Angle - MPI
  - Ray - OpenMP

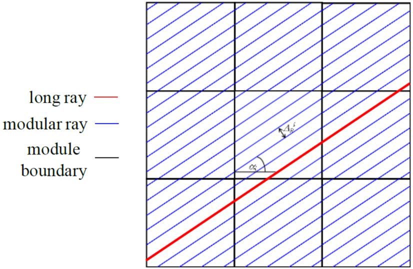

- Nodes must be axially homogeneous
- Control rod positions often do not align with node boundaries, requiring homogenization of control rod and moderator
- Volume homogenization preserves material volume/mass, but not reaction rates
- Two approaches to prevent rod cusping:
  - Refine mesh to align with all control rod positions
  - Decusping method to improve homogenization

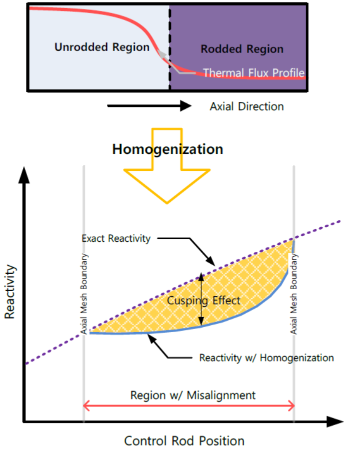

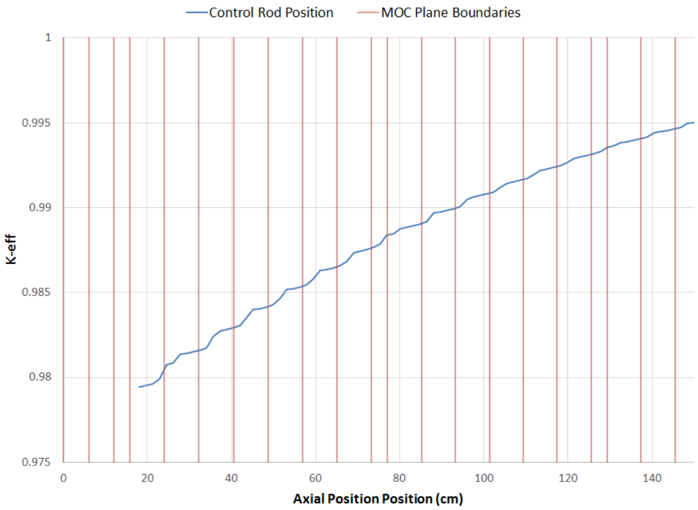
Control Rod Position
MOC Plane Boundaries
1
0.995
0.99
0.985
0.98
0.975
K-eff
0
20
40
60
80
100
120
140
Axial Position Position (cm)

Methods Shortcomings

- Extensive research has been done on decusping methods, primarily for nodal codes
- Several methods have been developed for 2D/1D codes
  - Some methods involved coarse approximations with limited accuracy
  - Others required expensive additional calculations that increased runtime of the code significantly
- New methods need to improve on prior ones by providing more accurate solutions without significantly slowing down calculations

Description

- Rodded 3×3 assembly case used to plot generate correction factors based on rod position
  - One set of calculations performed with refined mesh to eliminate cusping effects
  - Second set done with coarse mesh
  - Percent change in k_{eff} plotted against percent change in volume fraction for each set of calculations
  - Difference in curves used to reduce volume fraction during rod homogenization to reduce cusping effects
- Sixth order polynomial curves generated for AIC, B_4C, and tungsten rods

Polynomials

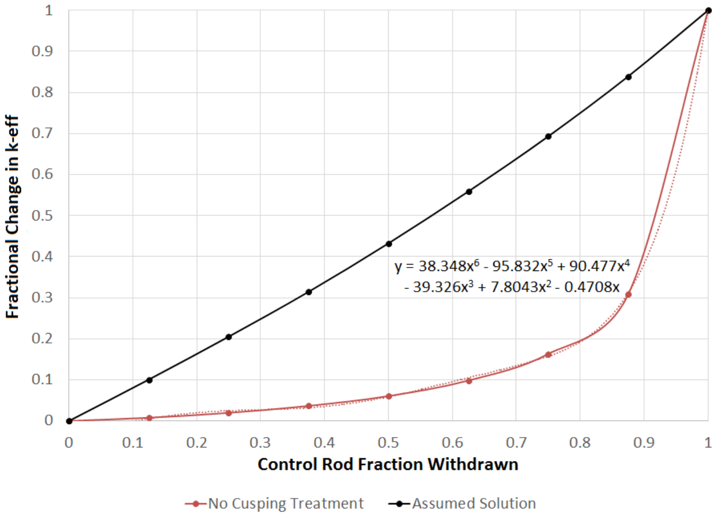

Subplane Decusping

- Modifications made to subplane scheme [9, 10] to treat axial effects of rod cusping
  - Homogenization still uses MOC flux with axial shape factor, but with heterogeneous rodded or unrodded cross sections
  - Projection rehomogenizes cross sections in partially rodded nodes after CMFD calculation

$$\overline{\Sigma_i} = \frac{\phi^R_{rad,i}\phi^R_{ax,i}\Sigma^R_i h^R + \phi^U_{rad,i}\phi^U_{ax,i}\Sigma^U_i h^U}{\phi^R_{rad,i}\phi^R_{ax,i} h^R + \phi^U_{rad,i}\phi^U_{ax,i} h^U}$$

Collision Probabilities Decusping

- Sub-plane modifications only capture axial effects
  - MOC uses homogenized cross section
  - Radial shape does not accurately reflect either region
- 1D collision probabilities (CP) introduced to generate radial shapes
  - Generates radial flux profile for rodded and unrodded region
  - Radial profiles used in CMFD homogenization
  - Fast calculation

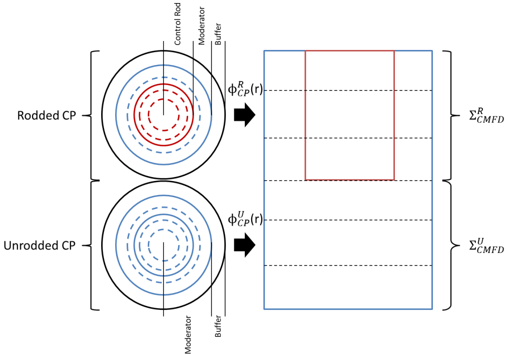

Description

- Other methods do not correctly address the MOC calculation
  - Homogenized cross sections are still used for 2D MOC
  - Flux shape from MOC does not accurately represent rodded or unrodded flux
- To improve MOC solutions, heterogeneous cross sections and sources must be accounted for
- MOC rays can be split into subrays in the vicinity of partially rodded regions
- Because of exponentials in MOC solution, rays can be recombined after rod

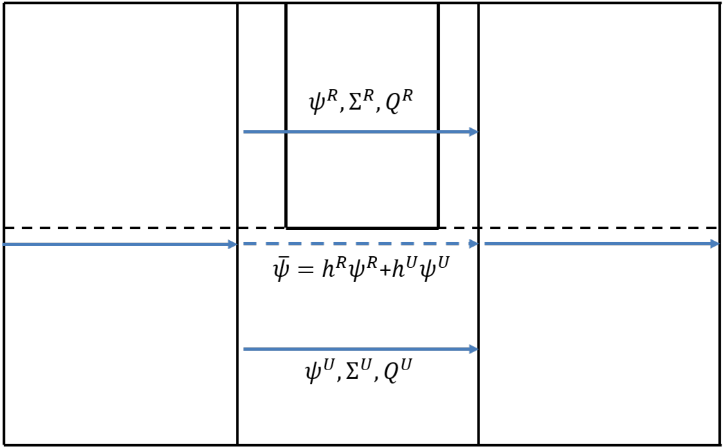

ψ^R, Σ^R, Q^R
$\bar{\psi} = h^R\psi^R + h^U\psi^U$
ψ^U, Σ^U, Q^U

2D/1D Modifications

- New MOC sweeper that duplicates long rays using axial volume fractions to average rays together
- Fluxes, cross sections, and sources stored for subregions that subrays pass through
- CMFD projection used to calculate subregion fluxes and generate subregion sources
- Subplane CMFD/P_3 results used to calculate axial TL sources in subregions
- Option added to control how far away from rod subray continues to be used

Recombination

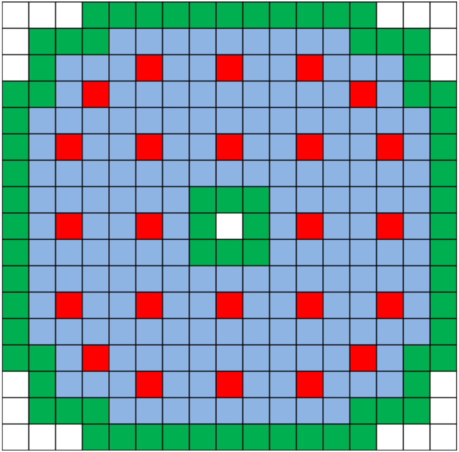

- Say some stuff about Watts Bar
- Say some stuff about c5g7

Problem Description

- Center 3x3 assembly cluster in Watts Bar Unit 1
- AIC control rod in center assembly placed at 257.9 cm
- Test cases used 57 planes, with rod inserted 50% into a plane
- Reference used 58 planes, with extra plane boundary aligned with rod tip
- All simulations used 1 core per plane

2.1	2.6 20 PY	2.1
2.6 20 PY	2.1 RCCA	2.6 20 PY
2.1	2.6 20 PY	2.1

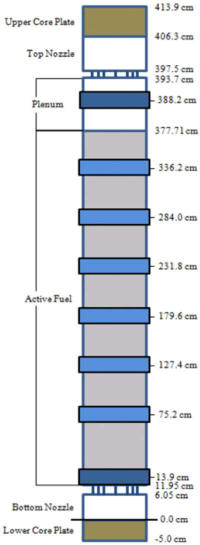

Test Procedures

- Differential rod worth curves were generated with fine mesh, coarse mesh, and each decusping method
- Comparison of curves shows effectiveness of decusping methods as rod is withdrawn through core
- KENO-VI was used to calculate reference solutions at 10% intervals
  - 500 inactive generations (Need to update keno comparisons)
  - 10,000 active generations
  - 5×10^6 particles per generation

Differential Rod Worth Curve

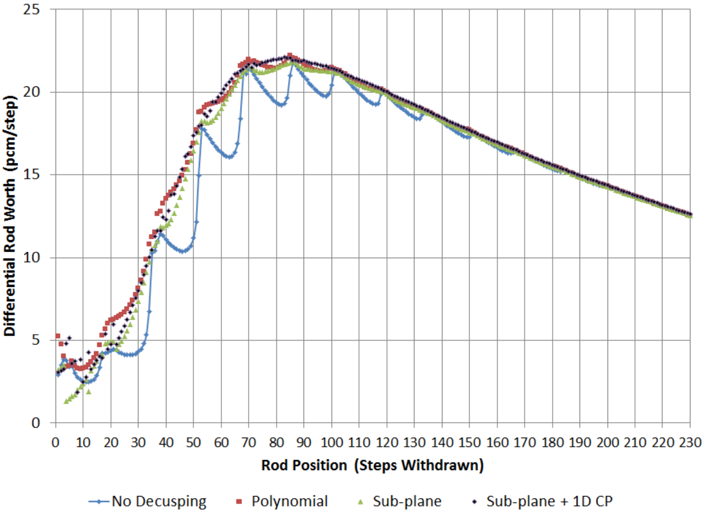

KENO-VI Comparisons

Cases	Decusping Method	k_{eff} Difference	Pin Power Difference RMS	Pin Power Difference Max
Average	None	−24.9	5.380%	25.902%
	Polynomial	34.8	1.502%	8.957%
	Subplane	34.6	0.984%	4.597%
	Subplane + CP	41.4	0.763%	3.386%
Worst – 20%	None	−176.0	14.709%	63.929%
	Polynomial	13.9	3.344%	25.373%
	Subplane	9.6	1.921%	9.900%
	Subplane + CP	45.9	1.324%	4.921%
Fully Withdrawn	–	40.5	0.34 %	1.493%

Problem Description and Test Procedures

- Bank D inserted to 257.9 cm, other banks all out
- 57 planes for tests and 58 for reference, 16 cores per plane

	H	G	F	E	D	C	B	A
8	2.1	2.6 20	2.1	2.6 20	2.1	2.6 20	2.1	3.1 12
9	2.6 20	2.1	2.6 24	2.1	2.6 20	2.1	3.1 24	3.1
10	2.1	2.6 24	2.1	2.6 20	2.1	2.6 16	2.1	3.1 8
11	2.6 20	2.1	2.6 20	2.1	2.6 20	2.1	3.1 16	3.1
12	2.1	2.6 20	2.1	2.6 20	2.6	2.6 24	3.1	
13	2.6 20	2.1	2.6 16	2.1	2.6 24	3.1 12	3.1	
14	2.1	3.1 24	2.1	3.1 16	3.1	3.1		
15	3.1 12	3.1	3.1 8	3.1				

Enrichment
Number of Pyrex Rods

	H	G	F	E	D	C	B	A
8	D		A		D		C	
9						SB		
10	A		C				B	
11				A		SC		
12	D				D		SA	
13		SB		SD				
14	C		B		SA			
15								

Problem 5 Results

Case	k_{eff} Difference (pcm)	Pin Power Differences RMS	Pin Power Differences Max	Iterations 2D/1D	Iterations CMFD	Runtime (Core-Hours)
Reference	–	–	–	13	481	361.7
No Treatment	-22	6.90%	30.55%	13	523	410.7
Polynomial	-5	1.15%	4.85%	13	463	373.7
Subplane	-5	2.09%	10.20%	13	499	399.0
Subplane + CP	-1	0.50%	2.74%	13	529	425.6

- Maximum error for each comparison occurs in pins neighboring the partially rodded pin cell

Problem Description

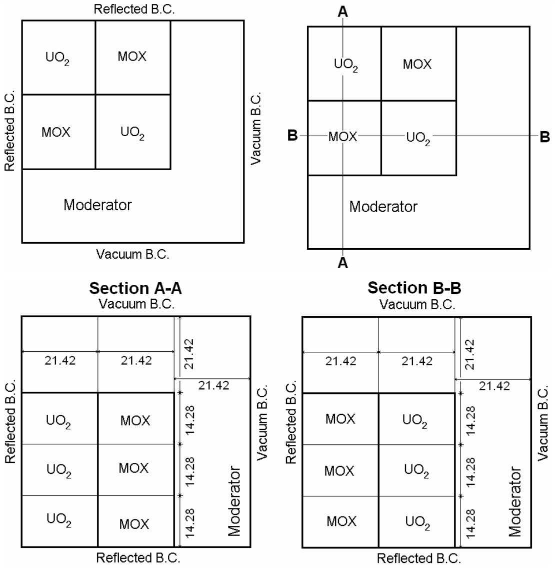

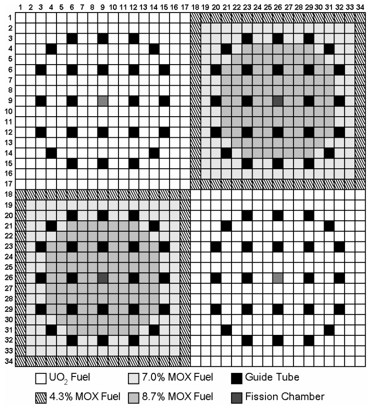

Test Procedure

- Three different C5G7 problems were simulated: 2D core, 3D assembly, and 3D core
- Rod was withdrawn through each problem in 1 cm increments for subray MOC and subplane methods
- k_{eff} and 3D pin power comparisons were made against a fine mesh reference solution at each position

2D Core Results

Rod Position	Reference k_{eff}	Subray-0 k_{eff}	Subray-0 Pin Powers RMS	Subray-0 Pin Powers Max	Subray-1 k_{eff}	Subray-1 Pin Powers RMS	Subray-1 Pin Powers Max	Subray-2 k_{eff}	Subray-2 Pin Powers RMS	Subray-2 Pin Powers Max	Subray-3 k_{eff}	Subray-3 Pin Powers RMS	Subray-3 Pin Powers Max
1*	1.06839	-15	0.10%	0.29%	-15	0.10%	0.29%	-15	0.10%	0.29%	-15	0.10%	0.29%
2	1.07746	-33	0.22%	0.67%	-34	0.22%	0.68%	-34	0.22%	0.67%	-34	0.22%	0.67%
3	1.08777	-53	0.32%	1.03%	-56	0.34%	1.07%	-55	0.34%	1.06%	-55	0.34%	1.06%
4	1.09919	-72	0.41%	1.34%	-78	0.45%	1.45%	-78	0.45%	1.44%	-78	0.45%	1.44%
5	1.11160	-89	0.46%	1.53%	-99	0.51%	1.69%	-98	0.50%	1.66%	-98	0.50%	1.66%
6	1.12495	-102	0.49%	1.66%	-115	0.55%	1.83%	-115	0.54%	1.82%	-115	0.54%	1.81%
7	1.13925	-112	0.49%	1.70%	-127	0.55%	1.88%	-126	0.55%	1.87%	-126	0.55%	1.86%
8	1.15469	-117	0.47%	1.65%	-133	0.53%	1.83%	-132	0.53%	1.81%	-132	0.52%	1.81%
9*	1.17190	-117	0.43%	1.50%	-127	0.46%	1.61%	-126	0.46%	1.60%	-126	0.46%	1.60%
Average	–	79	0.38%	1.26%	87	0.41%	1.37%	87	0.41%	1.36%	87	0.41%	1.36%

2D Core Results

Rod Position	Reference k_{eff}	Subray-0 k_{eff}	Subray-0 Pin Powers RMS	Subray-0 Pin Powers Max	None k_{eff}	None Pin Powers RMS	None Pin Powers Max	Subplane k_{eff}	Subplane Pin Powers RMS	Subplane Pin Powers Max	Subplane + CP k_{eff}	Subplane + CP Pin Powers RMS	Subplane + CP Pin Powers Max
1*	1.06839	-15	0.10%	0.29%	-286	1.73%	4.47%	-87	0.52%	1.35%	-169	0.99%	2.46%
2	1.07746	-33	0.22%	0.67%	-811	4.75%	12.70%	-198	1.13%	3.06%	-174	0.97%	2.57%
3	1.08777	-53	0.32%	1.03%	-1369	7.71%	21.30%	-290	1.56%	4.42%	-181	0.97%	2.70%
4	1.09919	-72	0.41%	1.34%	-1918	10.33%	29.42%	-360	1.83%	5.35%	-185	0.94%	2.75%
5	1.11160	-89	0.46%	1.53%	-2400	12.25%	36.00%	-405	1.93%	5.84%	-184	0.88%	2.68%
6	1.12495	-102	0.49%	1.66%	-2738	13.12%	39.83%	-424	1.89%	5.89%	-174	0.78%	2.47%
7	1.13925	-112	0.49%	1.70%	-2820	12.55%	39.38%	-416	1.72%	5.52%	-155	0.65%	2.11%
8	1.15469	-117	0.47%	1.65%	-2478	10.08%	32.80%	-377	1.44%	4.76%	-124	0.48%	1.62%
9*	1.17190	-117	0.43%	1.50%	-1461	5.31%	18.00%	-300	1.06%	3.60%	-80	0.29%	1.00%
Average	–	79	0.38%	1.26%	1809	8.65%	25.99%	317	1.45%	4.42%	158	0.77%	2.26%

2D Core Performance

Method	Long Rays per Plane	Increase
Reference	88440	–
Subray-0	107400	21%
Subray-1	111792	26%
Subray-2	115264	30%
Subray-3	117920	33%

Method	Iterations	Runtime (s)	Speedup
Reference	25.7	1107	–
None	25.8	739	1.50
Subplane	26.7	725	1.53
Subplane + CP	26.9	695	1.61
Subray-0	26.4	861	1.29
Subray-1	25.9	881	1.26
Subray-2	26.1	920	1.21
Subray-3	26.1	938	1.18

3D Assembly Results

Case	Method	k_{eff} Diff.	Pin Powers RMS	Pin Powers Max
Average	None	2193	6.05%	10.95%
	Subplane	222	0.88%	1.64%
	Subplane+CP	114	0.45%	0.84%
	Subray-0	52	0.25%	0.54%
	Subray-1	56	0.25%	0.55%
	Subray-2	56	0.25%	0.54%
	Subray-3	56	0.25%	0.54%
Position 8	None	-91	2.88%	4.19%
	Subplane	-319	1.51%	2.66%
	Subplane + CP	-106	0.52%	0.89%
	Subray-0	-104	0.53%	0.94%
	Subray-1	-104	0.52%	0.94%
	Subray-2	-105	0.53%	0.98%
	Subray-3	-105	0.53%	0.98%

3D Assembly Results

Plot of max power differences by rod position

3D Assembly Performance

Method	Long Rays per Plane	Increase
Reference	29480	–
Subray-0	48440	64%
Subray-1	52832	79%
Subray-2	56304	91%
Subray-3	58960	100%

Method	Iterations	Runtime (s)	Speedup
Reference	27.5	490	–
None	27.8	361	1.36
Subplane	27.5	374	1.32
Subplane + CP	27.2	353	1.39
Subray-0	27.6	444	1.11
Subray-1	28.7	464	1.07
Subray-2	28.8	475	1.04
Subray-3	28.8	478	1.03

3D Core Results

Case	Method	k_{eff} Diff.	Pin Powers RMS	Pin Powers Max
Average	None	21	6.62%	29.30%
	Subplane	21	0.69%	3.47%
	Subplane+CP	21	0.34%	1.69%
	Subray-0	21	0.20%	1.06%
	Subray-1	25	0.20%	1.14%
	Subray-2	25	0.20%	1.11%
	Subray-3	21	0.20%	1.11%
Position 16	None	-1730	12.62%	55.69%
	Subplane	-183	1.08%	5.61%
	Subplane + CP	-76	0.45%	2.38%
	Subray-0	-46	0.30%	1.76%
	Subray-1	-54	0.35%	2.01%
	Subray-2	-53	0.34%	1.97%
	Subray-3	-53	0.34%	1.96%

3D Core Results

Plot of max power differences by rod position

3D Core Performance

Method	Iterations	Runtime (s)	Speedup
Reference	27.8	3256	–
None	28.2	2581	1.25
Subplane	29.1	2454	1.32
Subplane + CP	28.9	2454	1.32
Subray-0	28.8	2851	1.13
Subray-1	28.9	2920	1.11
Subray-2	29.1	2963	1.09
Subray-3	29.2	3009	1.08

- Problem of subgrid axial heterogeneity for planar synthesis methods was described
- Rod cusping was identified as most severe axial heterogeneity
- Three new methods developed to address this problem:
  - Polynomial decusping: Fast and simple to implement, limited accuracy
  - Subplane collision probabilities: minimal runtime increases, good accuracy
  - Subray MOC: complicated to implement efficiently, very good acccuracy
- Give some more details, but this is the general idea

Methods Improvements

- Polynomials: more rod materials
- Subplane collision probabilites: other solvers (2D r-z CP, 2D MOC pin cell solver, 3D MOC, etc.)
- Subray MOC: optimization, shielding, other stuff MPACT does already (Pn/parallelism), improvements to a couple approximations (constant radial shape for source calculations, radial current tallying on subplane mesh)

Applications

- 2D/3D
- Other Heterogeneities
- More problems

- This material is based upon work supported under an Integrated University Program Graduate Fellowship.
- This research was supported by the Consortium for Advanced Simulation of Light Water Reactors (www.casl.gov), an Energy Innovation Hub (http://www.energy.gov/hubs) for Modeling and Simulation of Nuclear Reactors under U.S. Department of Energy Contract No. DE-AC05-00OR22725.
- This research also made use of resources of the Oak Ridge Leadership Computing Facility at the Oak Ridge National Laboratory, which is supported by the Office of Science of the U.S. Department of Energy under Contract No. DE-AC05-00OR22725.
- This research made use of the resources of the High Performance Computing Center at Idaho National Laboratory, which is supported by the Office of Nuclear Energy of the U.S. Department of Energy under Contract No. DE-AC07-05ID14517.

- Others

Questions?

Transport-Corrected Scattering Approximation

- Modifies self-scatter and total cross-sections to account for anisotropy while performing isotropic calculations
- Neutron Leakage Conservation (NLC) Method: H-1

$$\Sigma_{s0,g\to g} = \Sigma_{s0,g\to g} + \frac{1}{3D_g} - \Sigma_{t,g}$$

- In-Scatter Method: B-11, C-12, O-16

$$\Sigma_{s0,g\to g} = \Sigma_{s0,g\to g} - \frac{1}{\phi_{1,g}} \sum_{g'=1}^{G} \Sigma_{s1,g'\to g}\phi_{1,g'}$$

- Out-Scatter Method: All other isotopes

$$\Sigma_{s0,g\to g} = \Sigma_{s0,g\to g} - \sum_{g'=1}^{G} \Sigma_{s1,g\to g'}$$

2D MOC

- Solve along a specific direction Ω_n

$$\mathbf{r}=\mathbf{r_0}+s\boldsymbol{\Omega}_n \Rightarrow \begin{cases} x(s) = x_0 + s\Omega_{n,x} \\ y(s) = y_0 + s\Omega_{n,y} \\ z(s) = z_0 + s\Omega_{n,z} \end{cases}$$

- Problem reduces from PDE to ODE that can be solved analytically

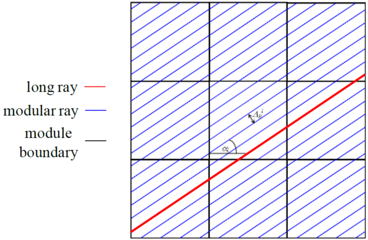

$$\frac{\partial \psi_{g,n}}{\partial s}+\Sigma_{t,g}(\mathbf{r}_0+s\boldsymbol{\Omega}_n)\psi_{g,n}(\mathbf{r}_0+s\boldsymbol{\Omega}_n)=q_{g,n}(\mathbf{r}_0+s\boldsymbol{\Omega}_n)$$

$$\psi_{g,n}(\mathbf{r}_0+s\boldsymbol{\Omega}_n) = \psi_{g,n}(\mathbf{r}_0)\exp\left(-\int_0^s \Sigma_{t,g}(\mathbf{r}_0+s'\boldsymbol{\Omega}_n)ds'\right) + \int_0^s q_{g,n}(\mathbf{r}_0+s'\boldsymbol{\Omega}_n)\exp\left(-\int_0^{s'} \Sigma_{t,g}(\mathbf{r}_0+s''\boldsymbol{\Omega}_n)ds''\right)ds'$$

2D MOC

- Assume flat source, cross-section along track with length L_j and spacing δx

$$\psi^{out}_{g,i,n,j} = \psi^{in}_{g,i,n,j} e^{-\Sigma_{t,g,i} L_j} + \frac{q_{g,i,n}}{\Sigma_{t,g,i}} \left(1 - e^{-\Sigma_{t,g,i} L_j}\right)$$

$$\overline{\psi}_{g,i,n,j} = \frac{q_{g,n,i}}{\Sigma_{t,g,i}} + \frac{1 - e^{-\Sigma_{t,g,i} L_j}}{L_j \Sigma_{t,g,i}} \left(\psi^{in}_{g,i,n,j} - \frac{q_{g,n,i}}{\Sigma_{t,g,i}}\right)$$

$$\overline{\psi}_{g,i,n} = \frac{\sum_j \overline{\psi}_{g,i,n,j} \delta x L_j}{\sum_j \delta x L_j}$$

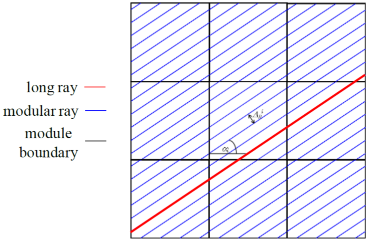

- Modular ray tracing can be used to minimize storage requirements by tracing only portions of problem geometry

2D MOC

- Perform ray tracing and store segment information up front
- Set up scattering, fission, and axial transverse leakage sources
    - Multi-group sweeping
    - 1-group sweeping
- Parallel Decomposition
    - Spatial (Planar and Radial)- MPI
    - Angle - MPI
    - Ray - OpenMP

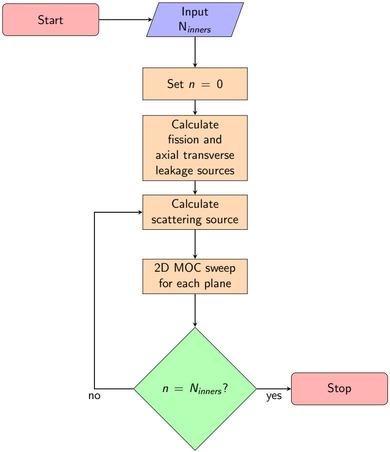

2D/1D Decusping Methods

- Neighbor Spectral Index Method - CRX-2K [11]
  - Spectral index is defined as the ratio of the fast flux to the thermal flux
  - Spectral index is used in top and bottom neighbor nodes to estimate partially rodded node flux profile
  - This estimate is used to update cross sections each iteration
- nTRACER Method [12]
  - Solves local problem to generate CMFD constants
  - Performs CMFD calculations on fine mesh to obtain axial flux profiles
  - Uses axial flux profiles during full core calculation to homogenize cross sections
- Approximate Flux Weighting Method [13]
  - Originally developed for nodal methods, but also implemented in nTRACER [14]
  - Assumes that in partially rodded node, rodded flux is similar to node above and unrodded flux is similar to node below
  - Assumption allows the partially rodded node cross section to be updated easily during iteration

J. Y. Cho *et al.*
"Three-dimensional heterogeneous whole core transport calculations employing planar moc solutions."
In: *Trans. Am. Nucl. Soc.*, volume 87, (pp. 234–236) (2002).

M. Hursin, B. Kochunas, and T. Downar.
DeCART Theory Manual.
Technical report, University of Michigan (2008).

H. G. Joo *et al.*
"Methods and performance of a three-dimensional whole-core transport code decart."
In: *PHYSOR 2004 – The Physics of Fuel Cycles and Advanced Nuclear Systems: Global Developments*. Chicago, Illinois (2004).

K. Smith.
"Nodal method storage reduction by nonlinear iteration."
Trans. Am. Nucl. Soc., **44**: p. 265 (1983).

R. G. McClarren.
"Theoretical aspects of the simplified pn equations."
Transport Theory and Statistical Physics, **39(2-4)**: pp. 73–109 (2011).

H. Finnemann, F. Bennewitz, and M. Wagner.
"Interface current techniques for multidimensional reactor calculations."
Atomkernenergie, **30(2)**: pp. 123–128 (1977).

J. Askew.
A characteristics formulation of the neutron transport equation in complicated geometries.
Technical report, United Kingdom Atomic Energy Authority (1972).

M. Halsall.
CACTUS, a characteristics solution to the neutron transport equations in complicated geometries.
Technical report, UKAEA Atomic Energy Establishment (1980).

A. M. Graham, B. S. Collins, and T. Downar.
"Improvement of the 2d/1d method using the sub-plane scheme."
In: *Proceedings of the International Conference on Mathematics and Computation (M&C 2017)*. Jeju, Korea (2017).

A. M. Graham, B. S. Collins, and T. Downar.
"Rod decusping techniques for the 2d/1d method."
In: *Proceedings of the International Conference on Mathematics and Computation (M&C 2017)*. Jeju, Korea (2017).

B. Cho and N. Z. Cho.
"A nonoverlapping local/global iterative method with 2-d/1-d fusion transport kernel and p-cmfd wrapper for transient reactor analysis."
Annals of Nuclear Energy, **85**: pp. 937–957 (2015).

Y. S. Jung and H. G. Joo.
"Control rod decusping treatment based on local 3-d cmfd calculation for direct whole core transport solvers."

In: *Proceedings of the International Congress on Advances in Nuclear Power Plants (ICAPP)* (2014).

J. C. Gehin.
A quasi-static polynomial nodal method for nuclear reactor analysis.
Technical report, Oak Ridge Inst. for Science and Education, TN (United States); Massachusetts Inst. of Tech., Cambridge, MA (United States) (1992).

M. Ryu and H. G. Joo.
"ntracer whole core transport solutions to c5g7-td benchmark."
In: *Proceedings of the International Conference on Mathematics and Computation (M&C 2017)*. Jeju, Korea (2017).